Cloud observations for the statistical evaluation of the UV index at Toowoomba, Australia

Cloud observations for the statistical evaluation

of the UV index at Toowoomba, Australia

A.V. Parisi[1,*], J. Sabburg[1], J. Turner[1] and P.K. Dunn[1]

[1]Faculty of Sciences, University of Southern Queensland, TOOWOOMBA. 4350.

AUSTRALIA. Fax: 61 74 6312721. Email: parisi@usq.edu.au

[*]To whom correspondence is to be addressed

Key words: clouds; UVI; UV index; erythemal; UV

Abstract

The development of a unique statistical model for the estimation of the UV index for all sky conditions with solar zenith angles of 60° or less is reported. The model was developed based on available data from an integrated whole-sky automated sky camera and UV spectral irradiance measurement system that was collected every five minutes when the equipment was operational over a period of one year. The final model does not include terms directly associated with solar radiation, but rather employs terms, and interactions between these terms, including the parameters of sky cover, solar obstruction, and cloud brightness. The correlation between the estimations of the model and the measured values was 0.81. The developed model was evaluated on a data set spanning five months that had not been employed in the development of the model. The correlation for this new data set was 0.50 which increased to 0.65 for the cases when the clouds were considered to be a contributor to UV enhancement above that of a cloud free day.

Introduction

For a given solar zenith angle (SZA), clouds are the largest influence on the solar UV (280 – 400 nm) irradiances on the earth's surface. Clouds can reflect, transmit, scatter and absorb the solar UV radiation. In addition to attenuation of the solar UV, clouds can also enhance the solar UV, depending on the configuration of the clouds and the relative position of the sun (Sabburg et al. 2003). Knowledge of the influences of clouds on the solar UV is required in order to employ models in the calculation of the solar UV for all sky conditions.

A series of studies have employed the measurement of parameters, such as the total solar radiation under all cloud conditions, to determine the modification of the measured total global solar UV irradiance compared to the corresponding clear-sky (i.e. cloudless sky) total global solar radiation (for example, Foyo-Moreno et al. 2003). The cloud cover was determined through the visual determination by trained observers. These authors developed a function that provided the modification of the UV based on the modification of the total global solar irradiance due to cloud. Foyo-Moreno et al. (2003) have developed an empirical model to estimate the solar UV that employs the optical air mass, the extraterrestrial solar UV and the measured global broadband hemispherical transmittance. A method to reconstruct the UV in the Netherlands has been reported that employs the reduction by cloud in the global broadband solar radiation to determine the UV exposures (den Outer 2005). Schwander et al. (2002) have integrated pyranometer broadband total solar irradiance and illuminance, measured by a Luxmeter, with the variables of SZA, ground albedo and cloud parameters. These were determined from visual observations of total cloud cover, cloud type (low, medium high and high) and solar disk obstruction, to determine the cloud modification factor (CMF) for the UV.

These authors found that a visual description of cloudiness was not adequate to determine CMFs. Integration of the broadband measurements provided deviations of mostly below 15% between the measured UV and the predicted UV.

CMFs have also been calculated by considering the relationship between the UV under all sky conditions to that under cloud free conditions for the same time period and atmospheric conditions (Foyo-Moreno et al. 2001). Visual observations of the cloud conditions for low-medium level clouds and high level clouds were employed and the CMF developed was the product of the CMF for each of the two different cloud categories.

Another series of studies employed direct cloud detection in order to establish relationships between different cloud parameters and the resulting UV irradiances. A number of these studies are reported in reviews of cloud effects on UV radiation by Calbó et al. (2005) and Parisi et al. (2004). Of particular interest to this current paper is the direct detection of clouds using automated sky cameras, to assist in estimating the UV index (UVI). Research by Sabburg and Wong (2000) came part way to achieving this. They used five sky parameters, obtained from a sun-centred sky camera (i.e. not a whole-sky camera as used in this current research), to develop a formula which, when used in conjunction with a clear-sky UV model, was found to have a coefficient of determination (the square of the correlation coefficient) of 82% compared to actual measured UV values. However, the formula was limited to cases of solar obstruction by cloud, the UVB spectrum and did not include cases of UV enhancement by cloud, i.e. UV levels exceeding the equivalent clear-sky value.

This current paper expands on the work done by Sabburg and Wong (2000), by including provision of all sky conditions, for the full UV spectrum, cases of UV enhancement and whole-sky assessment.

Materials and Methods

Cloud observations

The amount of cloud cover or sky cover was quantified with a Total Sky Imager (TSI) (model TSI-440, Yankee Environmental Systems, MA, USA) eliminating the issue of subjectivity that may be associated with observations by humans. The TSI was installed on a building roof at the University of Southern Queensland, Toowoomba, Australia (27.5 ^{o}S, 151.9 ^{o}E, 693 m above sea level). The site has relatively unpolluted skies. The system is configured to automatically collect data every five minutes for SZA less than 80°. Almost all of the sky is imaged and the analysis for cloud cover is performed on the image within a 160° field of view. A charge-coupled device **(**CCD) camera and software package capture 352 x 288 pixel, 24 bit, colour images into JPEG format data files, which are then analysed automatically by the TSI software for fractional sky cover (Figure 1). The operation of the instrument is based on a hemispherical reflective dome that points upwards on a horizontal plane. An image of the sky and clouds that is reflected on this dome is captured by a downward pointing CCD camera, suspended above and over the centre of the dome by a thin arm support. The portion of the sky near the horizon, in the part of the image that is not analysed, relates to approximately 12.5% of the sky. In order to prevent reflection of the sun and consequently possible damage to the CCD camera, a black shadow band is taped onto the reflective dome and the dome rotates to track the sun across the sky throughout the day using a software based almanac. This shadow band corresponds to approximately 9% of the image.

A detailed description of the TSI and most of the image analysis algorithms has been reported by Long et al. (2006). The parameters derived from the TSI that will be employed for the evaluation of the UVI for this current research are solar obstruction (SO), sky cover (CF), cloud uniformity (CU) and cloud brightness (CB). These are described as:

- *Solar obstruction,* provided as 1 if the sun was blocked by cloud and provided as 0 otherwise. This parameter has a major effect on the UVI, as UV radiation can be entirely diffuse radiation;

- *Sky cover,* the fraction of cloud cover provided as a fraction between 0 and 1. Cloud cover can attenuate UV radiation by over 50%, predominately by scattering processes, so this is another important variable to consider;

- *Cloud uniformity,* provided as a 0 or 1, namely 1 if the cloud amount in four quadrants is within 20% of total image, else 0. The four quadrants are defined as N to E, N to W, S to W and S to E. It has been found that the geometrical distribution of cloud can influence the amount of UV radiation received at the Earth's surface, so it is important that this variable is considered in the model.

- *Cloud brightness,* provided as 1 if the cloud in the image is considered by the TSI image analysis software to be a contributor to UV enhancement above that of a cloud free day, and else listed as 0. Scattering of visible light off cloud edges, and associated regions around the edges, is a good indication that UV enhancement has occurred. This should form part of any UVI model, as the UV radiation measured at the Earth's surface can exceed cloud-less sky values under these conditions.

It was not possible to classify cloud type, or estimate the cloud optical thickness. An existing software program calculated CB and CU for each TSI image. CF and SO were calculated by the standard TSI software for each image. The uncertainty in the determination of all parameters has been previously reported. The uncertainty in the determination of CF has been reported as ±10% at least 95% of the time (Sabburg and Long, 2004), CB and SO has been reported as ±28% (this parameter was previously called 'enhanced' by Sabburg and Long 2004), and ±15% (Long et al. 2006) respectively.

UV irradiances

The UV data was recorded with a UV spectroradiometer on an unshaded roof of a building at the University and located within five metres of the TSI. The spectroradiometer (model DTM300, Bentham Instruments, Reading, UK) is based on a double grating monochromator with a pair of holographic gratings with 2400 lines/mm. The instrument has been described elsewhere (Parisi and Downs 2004). Briefly, the instrument is installed in an air-tight container and scans the UV spectrum on a horizontal plane every five minutes from 280 to 400 nm at each 0.5 nm with a bandwidth of 0.5 nm. The temperature inside the container for each scan is recorded by the system software and the system is scheduled to automatically start scanning at 5:00 EST till 19:00 EST. Each scan, taking approximately two minutes, is initialised at 60 seconds before the five minute point with the collection of the UV spectrum starting at approximately each five minute point to coincide with the time when the TSI records a sky image. A correction for the dark count of each scan, or the electronic noise when no UV signal was entering the instrument, was determined during the initialisation and applied by the software to the spectral data. No correction was applied for the cosine error of the detector as the error associated with the cosine response of the diffuser was less than ±0.8% for a SZA up to 70° as provided by the manufacturer.

The data prior to January 2004 required application of a temperature correction based on the temperature coefficient for the anode sensitivity of -0.4%/^{o}C, provided by the manufacturer. The temperature coefficient for the wavelength shift provided by the manufacturer is 0.005 nm/^{o}C. The temperature change required to produce a shift of 0.1 nm is in excess of the temperature variation encountered and so the temperature coefficient for the wavelength shift was not corrected for. Post January 2004, the container housing the spectroradiometer was temperature stabilised and no temperature correction was required. The system was wavelength calibrated against the UV spectral lines of a mercury lamp and irradiance calibrated against a 150 W quartz tungsten halogen lamp calibrated to the National Physical Laboratory, UK standard. For the period of the data presented in this paper, the irradiance and wavelength calibrations were undertaken on 17 Mar 2003, 10 Dec 2003, 11 June 2004, 17 December 2004, 22 February 2005 and 6 May 2005. For the period of the data, the only interval that showed a drift in the instrument output between the calibration points, that was in excess of the uncertainty of the instrument, was between 11 June and 17 December 2004. This drift was -19% and for these six months, a linear interpolation of these percentage corrections was calculated between these two calibration points and the irradiance data corrected to account for the instrument drift between these calibration points. For all the other calibration points, the difference in the instrument output was within the uncertainty of the instrument and no correction was required.

The spectral UV data was weighted at each 0.5 nm with the erythemal action spectrum (CIE 1987), summed between 280 and 400 nm and multiplied by 0.5 in order to calculate the integrated erythemal UV irradiances with units of Wm^{-2}. Each of these irradiances

was converted to a UVI by multiplying by 40 (WMO 1994) for the development of the UVI model for the sky conditions encountered over the period of a year. The exposure categories for the UVI are low (< 2), moderate ($3 - 5$), high ($6 - 7$), very high ($8 - 10$) and extreme ($11 +$) (UNEP, 2007).

UVI model

The UVI data and concurrent cloud cover set, employed to develop the UVI model, consisted of spectral UV scans from 30 June 2003 to the end of December 2004, along with the associated processed TSI images, using the fully integrated measurement system. The daily total column ozone values were obtained for this location from the Total Ozone Mapping Spectrometer web site (TOMS 2005). These were valid for approximately 11:15 EST.

The cases where the SZA was less than or equal to 60° were employed in this paper in order to consider only the cases where the UV was greater and the related health implications were greater. At the latitude of the research, this corresponded to times between 9:45 EST and 14:05 EST at the winter solstice and 7:25 EST and 16:15 EST at the summer solstice. The smallest SZA encountered at the site was 4.1^{o} (US Naval Observatory 2006).

The first stage of the analysis was to determine the values of the UVI for the clear-sky cases, UVI_{clear}, for all SZA of 60° or less. Records where the TSI sky cover was less than 0.02 were considered in order to determine the clear-sky envelope. For these, records for which both CF < 0.99 and UVI ≤ 0.05 were removed as these may have been erroneous as they corresponded to cases where there was less than total cloud cover and UVI was almost zero. The data analysis for this and the remainder of this paper were undertaken

using R (R Development Core Team 2005). The range of total column ozone over the data period employed for the model development was 218 to 337 Dobson Unit (DU). The data was categorised according to the atmospheric ozone at the time into the three ozone ranges of 255 DU or less, 256 to 285 DU and 286 DU and higher, following a previously employed method (Sabburg and Parisi 2006).

A loess curve (Davison 2003) was fitted to the data in each ozone category. Loess curves are locally fitted curves, and are semi-parametric. They were used here to capture the fundamental relationship between sky cover and the ratio UVI/UVI_{clear} without undue influence from potential outliers in the data. A loess curve fits a curve to the data at point (x,y) using observations in the neighbourhood of the point, weighted by their distance from x. Here the neighbourhood (or the "span") consists of 75% of the points weighted with the tricubic weight $(1 - (distance/(maximum\ distance)\ )^3)^3$. The curve was then fitted to these observations using weighted least squares. This combination is the default in R, and provides a smooth curve through the points, yet still captures the relationship between the two variables. Varying the span produces similar results. After the loess curve was fitted, data points less than 1.5 below this fitted curve were omitted, with the value of 1.5 determined by visual inspection. Effectively, this omitted observations that were perhaps unusually low, and enabled the clear-sky envelope to be computed with greater certainty from the remaining observations. A quadratic equation was fitted to the UVI_{clear} data in each of the three categories using the technique of Sabburg and Parisi (2006). Although a cubic polynomial had previously been used by Sabburg and Parisi (2006), for this paper it was decided to use a quadratic polynomial (even though it had a slightly lower r^2 value), as it had a justifiable physical reason for its 'shape' (i.e. usually greater

cloud thickness is associated with greater cloud amount). Data points that were more than ±7% from the fitted quadratic for the corresponding SZA were omitted. This figure of ±7% is the uncertainty of the spectral UV data and any values that were more than this amount, from the fitted quadratic for the corresponding SZA, were considered to possess a UVI_{clear} category, primarily due to influencing factors (for example, aerosols) that were not detected by the TSI. A quadratic equation for each category was then fitted to the remaining UVI_{clear} data to produce the clear-sky envelopes.

A total of 8,346 data values were employed in the development of the model. For each data point, the ratio UVI/UVI_{clear} was calculated, where UVI is the measured UVI and UVI_{clear} is the value of the clear-sky envelope at the SZA of the measured value for the appropriate ozone range. The relationships of the four variables, CF, SO, CB and CU with the ratio UVI/UVI_{clear} were analysed. Care was taken not to overfit the model and P-values better than 0.01, and in some cases better than 0.001, were required in order to consider whether the parameter was significant.

Results

UVI model

The polynomials for the clear-sky envelopes for each of the ozone categories were found to be:

$UVI_{clear} = 24.92 - 0.4621.SZA + 0.001637.SZA^2$ (Ozone $\leq$ 255 DU)   (1)

$UVI_{clear} = 18.58 - 0.2604.SZA - 0.0001208.SZA^2$ (255 < Ozone $\leq$ 285 DU)   (2)

$UVI_{clear} = 18.52 - 0.3145.SZA - 0.0006586.SZA^2$ (Ozone > 285 DU)   (3)

These provide the clear-sky reference values for a particular SZA of 60° or less.

A sample TSI image, when the SZA was 51.5^o and the CF was 0.6, is shown in Figure 1, along with the associated solar UV spectrum measured at the time. A plot of the variation of the UVI/UVI_{clear} versus the sky cover is shown in Figure 2, for the five minute data. Figure 3 shows the UVI/UVI_{clear} versus CU, CB and SO. Within each box, the middle horizontal line represents the median. The box represents the upper quartile (Q3) and the lower quartile (Q1). The lines extend out of each box in both directions, an amount of 1.5*(Q3-Q1) past Q3 and Q1. The circles indicate observations that are more extreme than this.

The initial model that was tested contained terms with each of the variables CF, SO, CU, CB, terms with interactions between each of these four and a term in CF^2. The inclusion of the term in CF^2 was based on the results shown in Figure 2, which shows a possible quadratic relationship between UVI/UVI_{clear} and the sky cover. Figure 3 shows that there are differences between the values of UVI/UVI_{clear} for the two categories of CU and SO. Although, there did not appear to be a significant difference, shown in Figure 3, between the values of UVI/UVI_{clear} for the two categories of CB values, the CB term was retained at this point, in the event that interactions involving CB were found to be useful. The initial model tested was:

$$UVI/UVI_{clear} = \beta_o + \beta_1 SO + \beta_2 CF + \beta_3 CF^2 + \beta_4 CU + \beta_5 CB + \beta_6 CU.CB + \beta_7 CU.SO +$$
$$\beta_8 CF.CU + \beta_9 CF.CB + \beta_{10} CF.SO + \beta_{11} SO.CB \qquad (4)$$

where the last six terms are included to allow investigation of the interactions between each of the variables. The P-values for this model suggest that the terms containing CU, CU.CB, CU.SO and CF.CU are not significant. These terms were deleted, reducing the number of possible models to consider further. The model was then refined by considering terms involving CF^2. There are still many possible models available. Many of these models are very similar in statistical performance, and any one of these models could have been chosen. (To some extent the decision is a judgement based on comparing statistical performance measures and features in diagnostic plots.) The final model fitted to the data was:

$$UVI/UVI_{clear} = \beta_o + \beta_1 SO + \beta_2 CB + \beta_3 CF + \beta_4 CF^2 + \beta_5 CB.CF + \beta_6 SO.CF + \beta_7 CB.CF^2 + \beta_8 SO.CF^2 \qquad (5)$$

The adjusted R^2 value of 66.2% indicates the model explains 66.2% of the variance in the original data; the root mean-square error (RMSE) is 0.167. The values of the parameters of the fitted model are provided in Table 1, along with the standard error in each parameter and also the P-values. P-values are provided for both t-tests on the individual parameters and F- tests on the sequential models. F-tests are generally recommended for determining important predictors (for example, see Davison, 2003, Section 8.5). Because of the danger of over-fitting the model (given the large data set), variables were only retained if the corresponding P-value from the F-test was highly significant (P-value less than or equal to 0.0001). The only exception was the interaction between CB and CF, included since the interaction between CB and CF^2 was present in the model, as is common statistical practice. In any case, the P-value for this variable is still reasonably small.

13

The correlation between the estimations of this model and the measured values of UVI/UVI_{clear} was 0.81. Introducing a higher order term with CF^3 only marginally improved the fit to 0.82. Based on previous research (Sabburg and Wong 2000), the highest order CF term in the model was kept as CF^2.

Based on this model, for the cases of SO = 1 and CB = 0, the values of UVI/UVI_{clear} are less than the corresponding values for SO = 1 and CB = 1. The difference between these two cases increases as the CF increases. When CF > 0, the influences of cloud brightness are shown by UVI/UVI_{clear} being greater than 1 when CB = 1 and SO = 0. The ratio UVI/UVI_{clear} is not influenced as much by the CF when SO = 0 and CB = 0, compared to the cases when SO = 1. The value of -0.110 for the parameter of the SO.CF term shows that as CF increases the value of UVI/UVI_{clear} decreases due to this term, however the value decreases more dramatically due to the value of -0.557 for the parameter of the $SO.CF^2$ term. Note there is a strong correlation between SO and CF (0.67), so changes in one of these two parameters imply changes in the other; the discussion above should be read in this context.

Evaluation of the UVI model

The model described above in Equation (5) was subsequently evaluated on a dataset that had not been used in the development of the model (namely from 4 January 2005 to 30 May 2005). After applying the same quality assurance on the data, as was used in the previous dataset, a total of 5,514 scans remained. This dataset had a SZA range of 5.1 to 60°, ozone range of 235 to 285 DU, and contained 1,250 cases of solar obstruction and four cases of UV enhancement (these enhancements were based on the same clear-sky

envelopes as reported previously in Equations (1) to (3), with a UV index greater than 20%).

When the modelled UV index ratio data was correlated with the measured UV index ratio data (i.e. measured UV divided by the corresponding clear-sky envelope based on ozone, that was determined in the development of the model, namely Equations (1) to (3)) as shown in Figure 4, a coefficient of determination of 50% was obtained for a linear-fit to the data. The Figure only shows positive values of the modeled UVI as any negative values do not have a physical meaning. Only slight improvements to this correlation were found when looking at subsets of the data, including solar obstructed, not UV enhanced and limited SZA ranges. However, the highest correlation coefficient of determination of 65% was obtained for a subset of the data which only contained cases of bright cloud (i.e. CB equal to one), resulting in 2,046 scans.

As a measure of the model performance, the mean bias error (MBE) was measured, defined as

$$MBE = \frac{1}{n}\sum_{i=1}^{n} \hat{y}_i - y_i \tag{6}$$

where, in this situation, $\hat{y}_i$ is the UVI ratio predicted by Equation (5), y_i is the measured UVI ratio, and n is the length of the series. Usually the MBE is computed and compared for various subsets of the data, when large differences indicate bias in the results for various subsets. Here, the MBE was computed for both levels of SO and CB, and for four ranges of CF to ensure there was no systematic bias with CF. The results are reported in Table 2, showing in all cases small mean bias when the model is applied to the new data set.

Discussion

This paper has reported on the development of a unique model for the estimation of the UVI for all sky conditions encountered at Toowoomba, Australia with SZA of 60° or less, based on the cloud parameters derived from an all-sky camera. This is important as the modification due to clouds in the UVI forecast representing the maximum expected UV that is reported daily in the media, can now be determined by employing information on the cloud conditions at that time of the day.

An integrated whole-sky automated sky camera and UV irradiance measurement system was employed. Although the fractional sky cover could change over the time taken for the UV spectral scan, the time for the scan was made as short as possible, at approximately two minutes, in order to minimise this. The developed model employed the cloud parameters of sky cover, solar obstruction and cloud brightness. The correlation between the estimations of the model and the measured values was 0.81.

The developed model was evaluated on a data set spanning five months that had not been employed in the development of the model. The correlation for this new data set was 0.50 which increased to 0.65 for the cases when CB equalled one. The increase to 0.65, for the cases when CB equalled one, seems to indicate that increased visible radiation correlates well with the modelled UV radiation. It should be noted that as this is a purely statistical model, its use should be limited to the current location where the data was obtained, however, a similar methodology can be applied at any given location. The correlation found by Sabburg and Wong (2000), at this same location, was 0.82. The current study would appear to compare favourably with this when it is considered that for the current study, the clear-sky envelopes were based on measured data rather than UV modelled

data and the study by Sabburg and Wong (2000) included a normalisation factor in both the developed and evaluated datasets, and was limited to the UVB waveband. Also, in the earlier study some data points were removed based on manual intervention, where as in this current paper no selective deletion of suspect data points occurred. Finally, in the current model, only three parameters were available or found significant, compared to five parameters in the previous study (which was representative of a smaller field of view around the sun).

This current work utilised an off the shelf whole-sky automated sky camera, as opposed to the specialised sky camera developed by Sabburg and Wong (2000). Previous papers have considered the cloud parameters from manual observations of the cloud conditions and others have considered the impact of cloud on daily totals of UV exposures or exposures integrated over a longer period. The integrated whole-sky automated sky camera and UV irradiance measurement system presented in this paper has the advantage that short term variations in the cloud cover conditions, that are important for the effect on damaging responses to humans, can be investigated.

Previous research, based on manual observations, has established that for cloud fractions less than 0.5 (4 okta), the attenuation of UV by cloud is independent of the cloud type, whereas for cloud fractions of 0.87 or greater (7 and 8 okta), there is a large difference in the attenuation of UV by high level clouds and by cumulus clouds (Thiel et al. 1997). This implies that the estimation of the UVI, as developed by employing an integrated whole-sky automated sky camera and UV irradiance measurement system, can be improved in future research, by cloud classification and/or cloud optical thickness estimates. Whether using additional parameters derived from specialised, or off the shelf

whole-sky cameras, future research could also include the development of algorithms to differentiate cloud types and possibly altitude from sky images, and the incorporation of this information in the estimation of the UVI. An additional improvement may also be obtained by decreasing the time to acquire the UV irradiance data and thus reducing the variation in the cloud conditions for each irradiance data point.

References

Calbó J, Pages D, Gonzalez JA (2005) Empirical studies of cloud effects on UV radiation: A review. Reviews of Geophys 43 Art. No. RG2002:1-28

CIE (International Commission on Illumination) (1987) A reference action spectrum for ultraviolet induced erythema in human skin. CIE J 6:17-22

Davison AC (2003) Statistical models, Number 11 in Cambridge series in statistical and probabilistic mathematics, Cambridge University Press, UK

Den Outer PN, Slaper H, Tax RB (2005) UV radiation in the Netherlands: Assessing long-term variability and trends in relation to ozone and clouds. J Geophys Res 110:D02203 doi:10.1029/2004JD004824

Foyo-Moreno I, Vida J, Alados-Arboledas L (1999) A simple all weather model to estimate ultraviolet solar radiation (290-385 nm). J Appl Meteorol 38:1020-1026

Foyo-Moreno I, Alados I, Olmo FJ, Vida J, Alados-Arboledas L (2001) On the use of a cloud modification factor for solar UV (290-385 nm) spectral range. Theor Appl Climatol 68:41-50

Foyo-Moreno I, Alados I, Olmo, FJ, Alados-Arboledas L (2003) The influence of cloudiness on UV global irradiance (295-385 nm). Agric For Meteorol 120:101-111

Long CN, Sabburg JM, Calbó J, Pagès D (2006) Retrieving cloud characteristics from ground-based color all-sky images. J Tech 23:633-652

Parisi AV, Downs N (2004) Cloud cover and horizontal plane eye damaging solar UV exposures. Int J Biomet 49:130-136

Parisi AV, Sabburg J, Kimlin MG (2004) Scattered and Filtered Solar UV Measurements. Kluwer Academic Publishers, Dordrecht

R Development Core Team (2005) R: A language and environment for statistical computing, R Foundation for Statistical Computing. Vienna, Austria, ISBN 3-900051-07-0.

Sabburg J, Wong J (2000) Evaluation of a sky/cloud formula for estimating UV-B irradiance under cloudy skies. J Geophy Res 105(D24):29,685-29,692

Sabburg JM, Parisi AV, Kimlin MG (2003) Enhanced spectral UV irradiance: a one year preliminary study. Atmos Res 66:261-272

Sabburg J, Long CN (2004) Improved sky imaging for studies of enhanced UV irradiance. Atmos Chem Phys 4:2543-2552

Sabburg J, Parisi AV (2006) Spectral dependency of cloud enhanced UV irradiance. Atmos Res 81:206-214

Schwander H, Koepke P, Kaifel A, Seckmeyer G (2002) Modification of spectral UV irradiance by clouds. J Geophys Res 107(D16):4296 doi:10.1029/2001JD001297

Thiel S, Steiner K, Seidlitz HK (1997) Modification of global erythemally effective irradiance by clouds. Photochem Photobiol 65:969-973

TOMS, Total Ozone Mapping Spectrometer, NASA, http://toms.gsfc.nasa.gov/eptoms/ep_ovplist_a.html (accessed on Oct 2005)

UNEP (United Nations Environmental Programme), Global Solar UV Index, http://www.unep.org/PDF/Solar_Index_Guide.pdf (accessed on Mar 2007)

US Naval Observatory, Sun or Moon Altitude/Azimuth Table for One Day, http://aa.usno.navy.mil/data/docs/AltAz.html (accessed on Feb 2006)

WMO (World Meteorological Organization) (1994) Report of the WMO meeting of experts on UV-B measurements, data quality and standardization of UV indices, Les Diablerets, Switzerland, 25-28 July 1994, WMO/TD-NO. 625

Table 1 – Values for the parameters in the fitted model, along with the standard error for each parameter and also the P-value.

Variable	Parameter	Estimate	SE	t-test P-value	F-test P-value
Constant	β_0	0.968	0.007		< 0.0001
SO	β_1	-0.447	0.026	<0.0001	< 0.0001
CB	β_2	-0.021	0.010	0.032	< 0.0001
CF	β_3	0.168	0.040	<0.0001	< 0.0001
CF^2	β_4	-0.343	0.039	<0.0001	< 0.0001
CB.CF	β_5	0.611	0.088	0.024	0.0023
SO.CF	β_6	-0.110	0.049	<0.0001	< 0.0001
$CB.CF^2$	β_7	0.133	0.044	0.002	0.0001
$SO.CF^2$	β_8	-0.557	0.068	<0.0001	< 0.0001

Table 2 – The mean bias error (MBE) computed for various subsets of the data when the model is fitted to the new (evaluation) dataset. The MBE is computed separately for the subsets defined by each variable. CF has been (arbitrarily) divided into four parts.

Figure Captions

Figure 1 – Sample of a TSI image at a SZA of 51.5°, a CF of 0.6 and the associated UV spectrum at the time. The band in the image is the shadow band that tracks the sun and the thin line is the pole on which the camera is suspended.

Figure 2 – The UVI/UVI_{clear} ratio plotted versus the sky cover (CF) with a quadratic curve overlaid over the data.

Figure 3 – The UVI/UVI_{clear} ratio plotted against the cloud uniformity (CU), cloud brightness (CB) and solar obstruction (SO).

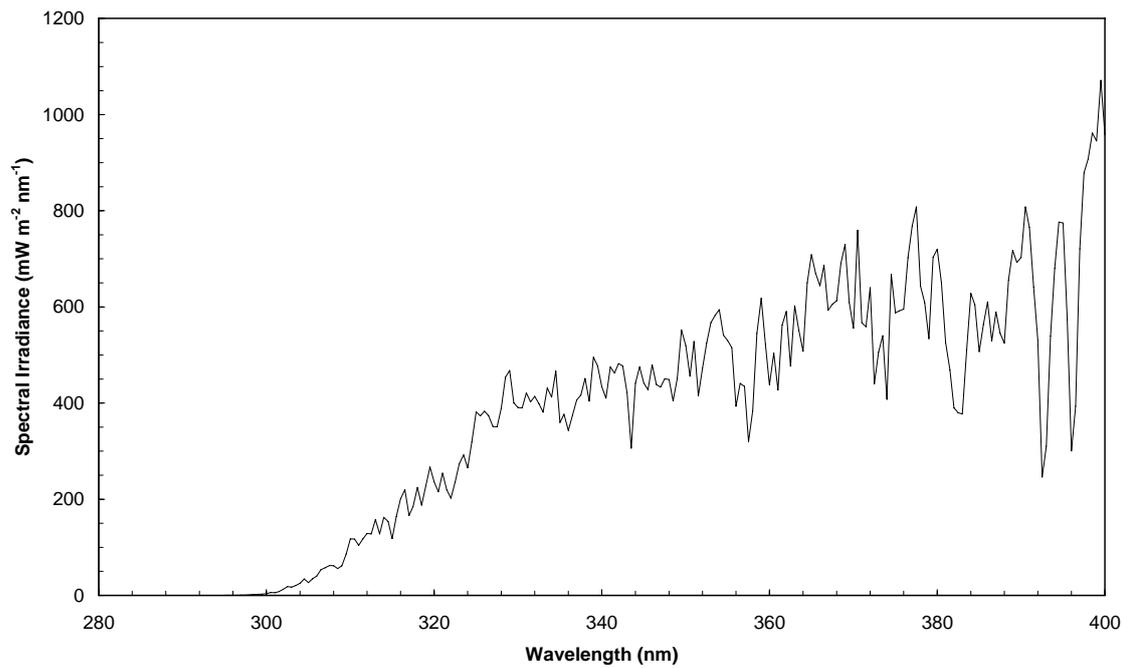Figure 4 – The modelled UVI ratio plotted against the measured UVI ratio for the new data set.

Figure 1 – Sample of a TSI image at a SZA of 51.5°, a CF of 0.6 and the associated UV spectrum at the time. The band in the image is the shadow band that tracks the sun and the thin line is the pole on which the camera is suspended.
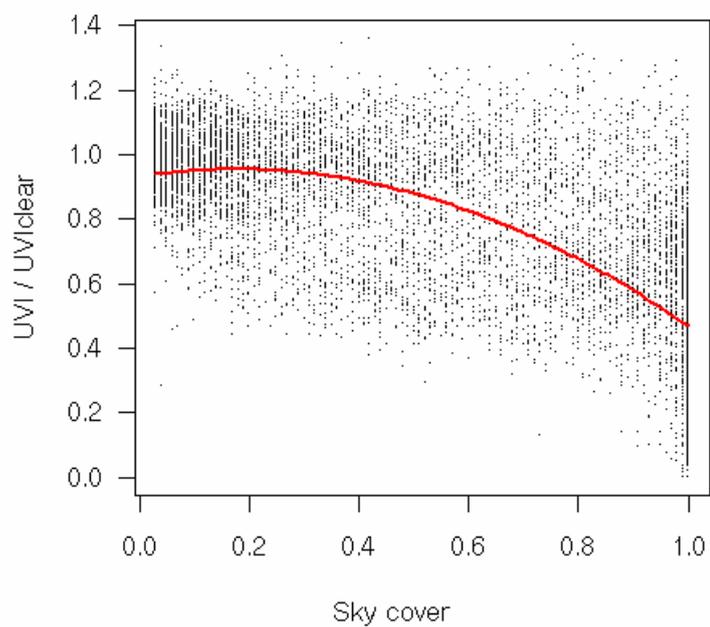
Figure 2 – The UVI/UVI$_{clear}$ ratio plotted versus the sky cover (CF) with a quadratic
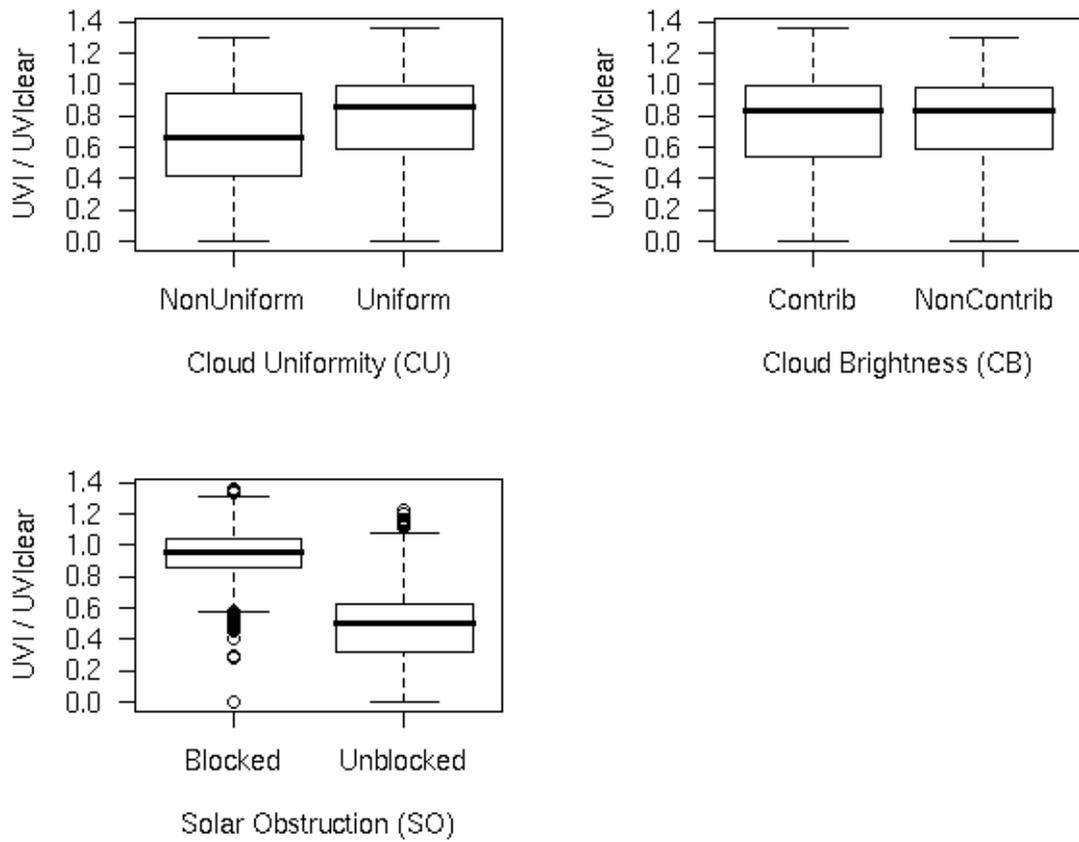curve overlaid over the data.

Figure 3 - The UVI/UVI$_{clear}$ ratio plotted against the cloud uniformity (CU), cloud brightness (CB) and solar obstruction (SO).
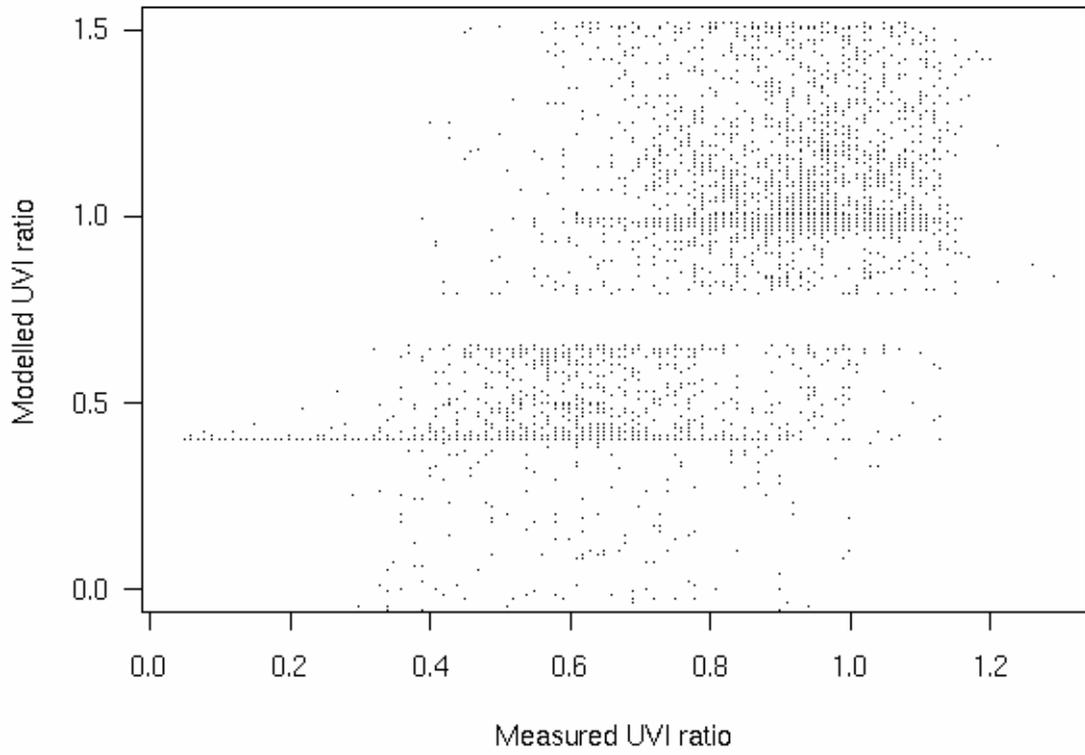
Figure 4 – The modelled UVI ratio plotted against the measured UVI ratio for the new
data set.